

pubs.acs.org/JPCC Article

Improved Structural Stability of Charged Hydrogels under Organic CO₂ Reduction Products: Effect of Acrylate and Methacrylate Backbone Linkages

Published as part of The Journal of Physical Chemistry virtual special issue "Early-Career and Emerging Researchers in Physical Chemistry Volume 2".

Jung Min Kim, Yi-hung Lin, Sean M. Bannon, Geoffrey M. Geise, and Bryan S. Beckingham*



Cite This: J. Phys. Chem. C 2023, 127, 10826–10832



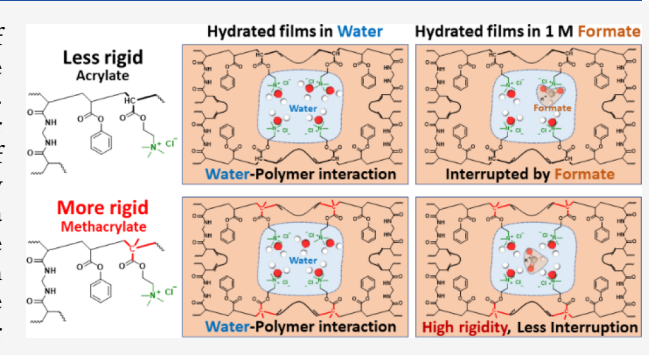
ACCESS

III Metrics & More

Article Recommendations

s Supporting Information

ABSTRACT: Understanding the mixed solute transport behavior of CO₂ reduction products (methanol and formate) in ion exchange membranes (IEMs) is of interest for CO₂ reduction cells (CO₂RCs). The role of an IEM in a typical CO₂RC is to suppress the crossover of all CO₂ reduction products while allowing the transport of electrolytes. Tuning the polymer rigidity of the membrane is a key contributor to such highly controlled transport of organic solutes in a dense hydrated membrane. Here, we investigate the mixed solute transport behavior of methanol and formate in a series of tough phenyl acrylate-based cross-linked IEMs. We then investigate the effects of a structural modification on mixed solute transport behavior by introducing quaternary carbons within the membrane. We



measured the relative permittivity properties of swollen films to determine if the water hydrogen bonding environment within the IEMs, which is related to maintaining selective ion transport within the membrane (electrolytes over CO₂ reduction products), was impacted by various organic solutes. We observed films with methacrylate backbone linkages have effectively constant relative permittivities when exposed to solutions containing methanol, formate, and a mix thereof. These findings may assist in designing membranes for applications, including CO₂ reduction cells and water—organic separation.

1. INTRODUCTION

Greenhouse gases (e.g., CO₂ and CH₄) are major contributors to climate change, and there have been significant efforts toward their capture, utilization, and storage. CO₂ reduction cells (CO₂RCs) are one promising technology to convert captured atmospheric CO₂ to valuable fuel sources (e.g., alcohols) and chemicals (e.g., carboxylates), enabling their utilization while simultaneously replacing fine chemicals traditionally sourced from petroleum. A CO₂RC often consists of three components: (1) cathode cell, (2) anode cell, and (3) ion exchange membrane (IEM).

A linear polymer-based anion exchange membrane (AEM) is often selected as the IEM to facilitate electrolyte (e.g., bicarbonate, HCO₃⁻) and hydroxide (OH⁻, from water oxidization) transport. Unfortunately, linear polymers often swell in the presence of alcohols such as methanol (MeOH^{3,4}), a polar organic sorbate and CO₂ reduction product, and isopropanol. Moreover, AEMs typically permit the crossover of carboxylates (CO₂ reduction products, e.g., formate (OFm⁻), a charged organic sorbate). Linear polymer-based cation exchange membranes (CEMs) have also been used, though less frequently, in CO₂RCs⁷⁻⁹ to facilitate the transport

of electrolytes (e.g., potassium, K⁺) and protons (H⁺, from water reduction). While linear polymer-based CEMs (e.g., Nafion 117³) are advantageous in suppressing the crossover of carboxylate anions, they still suffer from swelling in the presence of polar organic sorbates.³

Cross-linked polymer-based IEMs are one promising alternative to linear polymer-based IEMs (cross-linked sulfonated polysulfone¹⁰), as cross-links within the polymer network support the structural stability of the films and limit their swelling.^{10,11} However, several cross-linked films (e.g., cross-linked PEGDA-based IEMs^{6,12–14}) tend to have low toughness, which has limited their application. Recently, we developed a series of phenyl-based cross-linked IEMs by employing phenyl acrylate (PA) and phenyl methacrylate. We

 Received:
 March 20, 2023

 Revised:
 May 9, 2023

 Published:
 May 25, 2023





reported that the PA-based films had more favorable monomer solubility in solvent (i.e., DMSO) and Young's modulus than the phenyl methacrylate-based films. This manuscript thereby focuses in on the use of PA as the neutral comonomer and investigates the role of methacrylate vs acrylate backbone linkages for the ion exchange comonomers for both AEMs and CEMs.

Solute transport in polymeric membranes can often be explained by the solution-diffusion model, 15 where the membrane permeability (P_i) , a thickness and driving force normalized flux, can be expressed as a product of a sorption coefficient (K_{ν} which is sensitive to polymer-solute interactions¹⁶) and a diffusion coefficient (D_i, which is representative of the kinetic factors that contribute to the permeability¹⁵): $P_i = K_i \times D_i$. By measuring MeOH and KOFm diffusive permeabilities $(P_m \text{ and } P_f)$ via permeation cell experiments using both single and multisolute solutions, we aim to infer the efficacy of PA-based XL-IEMs (both AEMs and CEMs) in CO₂RC. Moreover, we performed sorptiondesorption experiments to measure the sorption coefficients, and we characterized the relative dielectric permittivity properties to investigate the polymer-solute-water interactions. Additionally, we evaluated the impact of polymer steric hindrance by replacing the acrylate with methacrylate on the backbone of the charged comonomer (Figure 1). We prepared

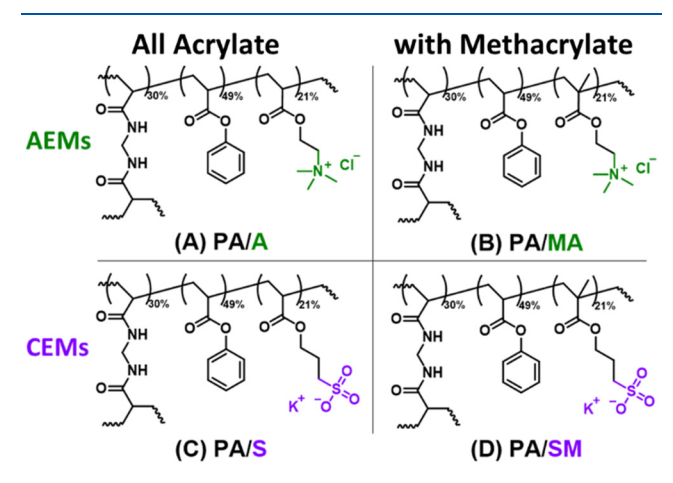


Figure 1. Scheme of prepared PA/A, PA/MA, PA/S, and PA/SM hydrogels.

four different films with two quaternary ammonium (QA+)containing monomers [2-(acryloyloxy)ethyl trimethylammonium chloride (AETAC, A) and 2-(methacryloyloxy)ethyl trimethylammonium chloride (MAETAC, MA)] and two sulfonate (SO₃⁻)-containing monomers [3-sulfopropyl acrylate potassium (SPAK, S) and 3-sulfopropyl methacrylate potassium (SPMAK, SM)], namely PA/A, PA/MA, PA/S, and PA/ SM. Among these charged monomers, AETAC (A) and SPAK (S) have acrylates in the backbone, and MAETAC (MA) and SPMAK (SM) have methacrylates in the backbone. In terms of the polymer chains, the methacrylate-containing films are more sterically constrained than the acrylate-containing films. 17 In the case of poly(methyl methacrylate) (PMMA) and poly-(methyl acrylate) (PMA), where the only difference is the presence of the methyl group on PMMA, the glass transition temperatures (T_g) differ by approximately 100 °C (105 °C for PMMA and 9 °C for PMA). Therefore, the chains are more rigid and less able to relax in response to changing solvent

conditions. Here, the difference in $T_{\rm g}$ is less pronounced (6–7 °C) in the final membranes (see Supporting Information Table S1 for $T_{\rm g}$ values) but follows a similar behavior with the methacrylate-containing films exhibiting higher $T_{\rm g}$ than the analogous acrylate-containing films.

2. METHODS

- 2.1. Materials. Phenyl acrylate (PA, 97%) was purchased from Ambeed, Inc. (Arlington Heights, IL). [2-(Acryloyloxy)ethyl]trimethylammonium chloride (AETAC, A, ca. 80% in water), 3-sulfopropyl acrylate potassium (SPAK, S), 3sulfopropyl methacrylate potassium (SPMAK, SM), and 2,2'azobis(2-methylpropionitrile) (AIBN, 98%) were purchased from Sigma-Aldrich Chemicals (St. Louis, MS). 2-(Methacryloyloxy)ethyl trimethylammonium chloride (MAE-TAC, MA, ca. 80% in water), and N,N'-methylenebis-(acrylamide) (MBAA, >98%) were purchased from TCI (Tokyo, Japan). Dimethyl sulfoxide (DMSO, ≥99.9%) was purchased from Macron Fine Chemicals (Radnor, PA). Type-1 deionized water (DI water) was produced by a Waterpro BT Purification System from Labconco (18.2 mΩ·cm at 25 °C, 1.2 ppb TOC) (Kansas City, MO). Feeler gauges (205 μ m, spacers) and glass plates $(5" \times 5" \times 0.25")$ were purchased from McMaster-Carr (Elmhurst, IL).
- **2.2. Membrane Preparation.** The detailed synthetic approach is described elsewhere. ^{11,19} Briefly, four transparent prepolymerization solutions were prepared by dissolving 30 mol % MBAA, 49 mol % PA, 21 mol % of a charged monomer (A, MA, S, or SM) and 0.1 wt % AIBN in DMSO (50 wt %). Each solution was transferred on a glass plate (5" × 5" × 0.25"), and two feeler gauges (205 μ m) were placed on two sides, carefully covered with an identical glass plate, and placed inside an oven at 60 °C for 8 h. Each film was placed in about 500 mL of DI water for 2 days to exchange DMSO to water.
- **2.3. Water Volume Fraction.** First, the dry polymer density, ρ_p , was calculated using an Archimedes principle method²⁰ with a density kit coupled with a scale (ML-DNY-43 and ML204T, Mettler Toledo (Columbus, OH)) as follows:

$$\rho_p = (\rho_L - \rho_0) \left(\frac{W_d}{W_d - W_L} \right) + \rho_0 \tag{1}$$

where ρ_L is the water density (997.8 kg/m³ at 22 °C), ρ_0 is the air density (1.225 kg/m³), W_d is the dried film weight in the air, and W_L is the film weight in auxiliary liquid (water), which was measured swiftly to minimize the water sorption into the gel. Next, the water volume fraction, ϕ_w , was calculated as follows:

$$\phi_{w} = \frac{(W_{s} - W_{d})/\rho_{L}}{(W_{s} - W_{d})/\rho_{L} + W_{d}/\rho_{p}}$$
(2)

where W_s is the hydrated film weight.

2.4. lonic Conductivity. In-plane ionic conductivities of all hydrated films were measured using an electrochemical impedance spectroscopy (EIS) potentiostat (Interface 1000E, Gamry Instruments (Warminster, PA)) with a four-point conductivity cell (BT-110, BekkTech (Loveland, CO)). The use of an in-plane conductivity measurement to inform what is ultimately a through-plane transport property was predicated on the assumption that these materials are sufficiently isotropic to consider the in-plane conductivity representative of the through-plane conductivity. The film was cut in a rectangular

shape (5 × 10 mm²) and placed on the conductivity cell, which was then placed in the DI water (0.5 L). EIS was performed within the range of 10 Hz to 1 MHz (AC voltage: 10 mV), the data were analyzed using an Echem Analyst software (Gamry Instruments), and the resistance (R, Ω) was obtained from the Nyquist plot by reading the real axis intercept. The ionic conductivity (σ , S/cm) was calculated as follows:

$$\sigma = \frac{L}{RWT} \tag{3}$$

where L is the distance between the electrodes (5 mm), W is the membrane width (5 mm), and T is the membrane thickness.

2.5. Young's Modulus. Young's moduli of all films were characterized using a commercial tensile test apparatus (RSA III dynamic mechanical analyzer, TA Instruments (New Castle, DE)). ¹¹ Each hydrated film was precut into rectangles $(10 \times 40 \times 0.2 \text{ mm}^3)$. The tensile test apparatus clamped the samples at both ends in the length direction, leaving 10 mm of starting length between the clamps. Tensile testing was triplicated by 0.05 mm/s deformation rate in ambient air (25 °C). Young's moduli were computed based on the initial slope of stress—strain curves.

2.6. Glass Transition Temperature. The glass transition temperature ($T_{\rm g}$) of each dry polymer film was measured using a TA Instruments Q20 DSC (Supporting Information Table S1). Approximately 10 mg of each film were sealed in an aluminum pan. All samples were equilibrated at $-50~{\rm ^{\circ}C}$ and ramped to 300 ${\rm ^{\circ}C}$ at 10 ${\rm ^{\circ}C/min}$. The $T_{\rm g}$ was determined from the thermogram where the temperature at the midpoint of the step change was taken as the $T_{\rm g}$.

2.7. Permeation Cell Experiment. The detailed approach is described elsewhere. 14 Briefly, MeOH and KOFm permeabilities of all membranes were measured in single and mixed solutes with a temperature-jacketed permeation cell coupled with an in situ attenuated total reflectance-Fourier transform infrared (ATR-FTIR) probe (9.5 mm AgX DiComp probe) with ReactIR15 (Mettler-Toledo) at 25 °C. Each hydrated film was cut with a 1-in. hole punch (1271M, General Tools (Secaucus, NJ)) and placed between the orifices of the feed and receiver cells. Next, the feed cell (25 mL) was filled with aqueous 1 M MeOH, 1 M KOFm, or a combined 1 M MeOH and 1 M KOFm solution. The receiver cell (25 mL) was filled with DI water, and the probe was placed in this cell. The permeability values (P_i) were then calculated with Yasuda's model, which derives from a pseudosteady state analysis of 1-dimensional Fickian diffusion in the membrane: 21,22

$$P_{i} = \ln \left(1 - \frac{2c_{i,l}(t)}{c_{i,0}} \right) \left(\frac{-lV}{2At} \right)$$
(4)

where i is a solute (either MeOH or KOFm), l is the membrane thickness, t is the time, $c_{i,l}$ (t) is the time-resolved solute concentration in the receiver cell (initially 0 M), $c_{i,0}$ is the initial concentration in the feed cell (1 M), V is the volume of each equivalent volume half-cell (25 mL), and A is the area of the orifice of the half-cell (1.1423 cm²). The impact of osmotic (water) diffusion was neglected, as the impact was found to be within the experimental error in a commercial CEM (Nafion 117^{23}).

2.8. Sorption–Desorption Experiment. The detailed approach is described elsewhere. ¹⁴ Briefly, the MeOH and

KOFm sorption coefficients for all membranes were measured in single and mixed solute sorption. Each hydrated film was cut with a 0.75-in. hole punch (1271I, General Tools) and placed in the sorption solution (4 M MeOH, 4 M KOFm, or 4 M of each solute) for 2 days, where the solution was replaced daily. The 4 M solute concentration was necessary due to detection limits inherent to the measurement. Next, the swollen film volumes (V_i, L) were calculated by measuring the film thickness (μ m) with a digital caliper ($\pm 1 \mu$ m) and the surface area (cm²) with a digital photograph and ImageJ software (National Institutes of Health, MD). The film surfaces were then blotted with tissue paper, and each film was placed in a desorption solution (initially 10 mL DI water), which was stirred for 2 days. Lastly, the desorption solution concentrations (M) were measured with a high-performance liquid chromatography (HPLC) setup, which consists of a refractive index detector and a column (Aminex HPX-87H column, Bio-Rad (Hercules, CA)). The solute content (n_i, mol) was calculated by multiplying the desorption solution concentration and the initial desorption solution volume (10 mL). Next, the solute concentration (C_i^m, M) in the membrane was calculated as $C_i^m = n_i/V_i$. Finally, the sorption coefficient (K_i) was calculated by dividing C_i^m by the sorption solution concentration $(C_i^s, 4 \text{ mol/L})$: $K_i = C_i^m/C_i^s$.

2.9. Microwave Dielectric Spectroscopy. The dielectric permittivity properties of the hydrated membranes were characterized by measuring the relative complex permittivity (ε^*) of the membrane samples in the microwave frequency range (45 MHz to 26.5 GHz). The measurements were made using a vector network analyzer (VNA, N9928A, Keysight (Santa Rosa, CA). The VNA was used to acquire membrane scattering parameters, which were then analyzed over the frequency range to determine the complex permittivity. The variation of the complex permittivity.

A coaxial transmission line sample holder (3.5 mm VNA Calibration Kit, 8043S5, Maury Microwave (Ontario, CA)) was used to make the measurements. All hydrated films were cut into 0.5 cm wide rectangular-shaped strips. Each sample was then wrapped tightly around the inner conductor of the sample holder to fill the annular space of the transmission line. Finally, the sample holder containing the hydrated film was connected to the VNA by shielded coaxial cables (N9910X0-708, Keysight Technologies).

To analyze the data, the complex permittivity was deconvoluted into its real and imaginary parts. 24,28 The real part of the relative complex permittivity is the relative permittivity (ε'), and the imaginary part of the relative complex permittivity is the dielectric loss (ε''). For hydrated membranes, the relative permittivity is often constant at frequencies lowers than 1 GHz and is effectively equal to the static dielectric constant of the hydrated sample. $^{25,26,29-31}$ Here, the dielectric constant in the low-frequency limit (i.e., the static dielectric constant) was taken as the value of the relative permittivity that was measured at 45 MHz.

3. RESULTS AND DISCUSSION

3.1. Water Volume Fraction. The water volume fraction (ϕ_w) of all films was measured in triplicate (Table 1). Generally, ϕ_w of sulfonate (SO_3^-) containing films (PA/S) and PA/SM) was higher than that of quaternary ammonium (QA^+) containing films (PA/A) and PA/MA. This result is likely due to the hydration number of sulfonate $(R-SO_3^{-32})$ being higher than that of ammonium (NH_4^{+33}) . Next, the

Table 1. Water Volume Fractions, Ionic Conductivities (Cl⁻Conductivity for PA/A and PA/MA and K⁺ Conductivity for PA/S and PA/SM), and Young's Moduli of All Films^a

	Water volume fraction, $\phi_{\scriptscriptstyle W}$	Ionic conductivity (mS/cm)	Young's modulus (MPa)
PA/A	0.39 ± 0.01	6.1 ± 0.1	0.87 ± 0.01
PA/MA	0.43 ± 0.00	6.0 ± 0.0	0.75 ± 0.03
PA/S	0.47 ± 0.00	10.6 ± 0.0	0.66 ± 0.01
PA/SM	0.50 ± 0.01	11.8 ± 0.0	0.62 ± 0.01

^aAll measurements were made at room temperature, and all values were measured in triplicate (standard deviations are reported).

methacrylate-containing films (PA/MA and PA/SM) had greater $\phi_{\scriptscriptstyle W}$ than the methacrylate-free films (PA/A and PA/S). Similarly, the hydrated film thicknesses of PA/MA and PA/SM were 150 and 153 μ m, respectively, and those of PA/A and PA/S were 130 and 137 μ m, respectively. Methacrylate-containing films are expected to experience less osmotic deswelling because of greater steric hindrance due to the quaternary (4°) carbons on the polymer backbone.

3.2. Ionic Conductivity. Chloride (Cl⁻) conductivities of QA+ containing AEMs (PA/A and PA/MA) and potassium (K⁺) conductivities of SO₃⁻ containing CEMs (PA/S and PA/ SM) were measured (Table 1). For CEMs, we assumed the ionic conduction is occurring primarily by K+. The conductivities of methacrylate-free and methacrylate-containing films were essentially unchanged for the AEMs and slightly elevated for the methacrylate-containing CEMs; $6.1 \approx 6.0 \text{ mS/}$ cm and $10.6 \approx 11.8$ mS/cm, respectively. These results indicate the methacrylates have a negligible to very small impact on the electromigration of both K⁺ and Cl⁻. Notably, these conductivity values might be affected if CO2 reduction products (MeOH and KOFm) are included in the measurement. For instance, the inclusion of formate ion $(K_b = 5.55 \times$ 10^{-11}) in solution will alter the pH of the potassium formate/ water solutions (8.9 for 1 M KOFm and 9.2 for 4 M KOFm).

The K⁺ conductivities of CEMs were higher than Cl⁻ conductivities of AEMs. This result is unexpected as the ionic mobilities of K⁺ and Cl⁻ are close (K⁺: $7.62 \times 10^{-4} \approx \text{Cl}^-$: $7.91 \times 10^{-4} \text{ cm}^2 \text{ s}^{-1} \text{ V}^{-1}$). A possible contribution to this behavior is the ϕ_w of CEMs being higher and, therefore, easier for K⁺ to migrate through the polymer network. Another possible contribution is the binding affinity of K⁺ to SO₃⁻ might be less than that of Cl⁻ to QA⁺.

3.3. Young's Modulus. Young's moduli of all films were measured in triplicate (Table 1); see Supporting Information Figure S1 for strain–stress curves. All films showed comparable Young's moduli to a commercial AEM (FAA, 2.0 MPa) and a commercial CEM (Nafion 117, 1.0 MPa), which we previously measured. Generally, Young's moduli values decrease as ϕ_w increases. A similar trend was observed in our previous investigation for analogous PA-based AEMs (PA/MA) and CEMs (PA/2-acrylamido-2-methylpropane sulfonic acid (PA/AMPS)). These trends indicate PA-based crosslinked films (prepared under similar conditions) with a lower ϕ_w likely undergo more deswelling during solvent exchange from DMSO to water which provides additional capacity for subsequent chain stretching.

3.4. MeOH and KOFm Permeability. MeOH permeabilities (P_m) and KOFm permeabilities (P_f) of all films were measured in single solute permeation $(P_{i,1})$ and mixed solute permeation $(P_{i,2})$ experiments (Figure 2, Supporting Informa-

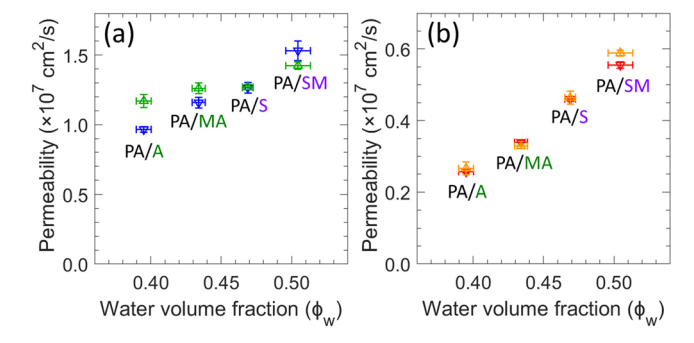


Figure 2. (a) MeOH permeabilities in single (blue) in mixed solute permeation with KOFm (green) and (b) KOFm permeabilities in single (red) in mixed solute permeation with MeOH (orange) as a function of water volume fraction.

tion Table S2). Generally, solute permeabilities were higher for the films with a larger $\phi_{\rm w}$ and when the smaller solute (MeOH) was considered. The kinetic diameter of MeOH (3.6 Å 34) is smaller than the hydrated diameters of K $^+$ (6.6 Å 35) and OFm $^-$ (HCO $_2^-$, > 5.9 Å 36,37). Continued discussion on the relative impacts of diffusion and sorption can be found in the next section.

The KOFm permeability values for all films were essentially unaffected by the presence or absence of MeOH in the measurement (Figure 2b). This result indicates that copermeating MeOH did not alter the overall KOFm permeabilities. In contrast, MeOH permeabilities in mixed solute permeation with KOFm $(P_{m,2})$ are different from those by itself $(P_{m,1})$, where $P_{m,2}$ of PA/A, PA/MA, PA/S, and PA/ SM are different from $P_{m,1}$ of these films by +21, + 9, 0, and -7%, respectively. These results indicate that copermeating KOFm alters the overall MeOH permeation. To explain these differences, we conjecture a potential relationship between the $\phi_{\scriptscriptstyle W}$ and the flux coupling ³⁸ (MeOH–KOFm). Assuming the average chain spacing within each film is proportional to $\phi_{\scriptscriptstyle W}$, the solute-solute interaction may be more likely as the chain spacing decreases (lower ϕ_w); therefore, the flux coupling is more likely to occur (more MeOH diffusion along with KOFm). However, the solute-solute interaction is less likely as the chain spacing increases (higher ϕ_w); therefore, the flux coupling is less likely to occur (less MeOH diffusion).

3.5. MeOH and KOFm Sorption Coefficients. MeOH sorption coefficients (K_m) and KOFm sorption coefficients (K_f) of all films were measured in single sorption $(K_{i,1})$ and mixed solute sorption $(K_{i,2})$ experiments (Figure 3, Supporting Information Table S3). Generally, MeOH sorption coefficients in single sorption $(K_{m,1})$ and mixed solute sorption with KOFm $(K_{m,2})$ were similar (Figure 3a). Based on the volume fraction of MeOH–KOFm–water–polymer within the swollen films, we observed more rigid films (PA/MA and PA/SM) had a higher MeOH fraction in cosorption with KOFm (17% and 14%, respectively) when less rigid films (PA/A and PA/S) had the same MeOH fraction in cosorption (Supporting Information Table S3). This result indicates MeOH is more favorable in rigid structures.

On the other hand, KOFm sorption coefficients were affected by the presence of MeOH. KOFm sorption coefficients in cosorption with MeOH were less than those measured by itself; $K_{f,2} < K_{f,1}$ (Figure 3b). Based on the volume fractions of MeOH–KOFm–water–polymer within the

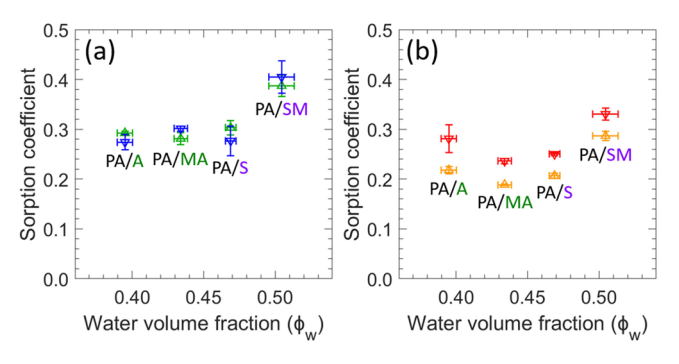


Figure 3. (a) MeOH sorption coefficients in single (blue) in mixed solute sorption with KOFm (green) and (b) KOFm sorption coefficients in single (red) in mixed solute sorption with MeOH (orange) as a function of water volume fraction.

swollen films, we observed the KOFm fraction decrease by 25%, on average (Table S4).

In addition, we also noticed the gaps between $K_{f,1}$ and $K_{f,2}$ were larger for QA⁺-containing films (PA/A, 22%, and PA/MA, 20%) than those of SO_3^- -containing films (PA/S, 17%, and PA/SM, 13%). As a conjecture, mobile formate anions (OFm⁻) may be more favorable in QA⁺-containing films (counterion condensation^{39,40}). In mixed solute sorption, OFm⁻ mobility can be reduced in these films as MeOH softens the fixed charge interface and interferes with the counterion condensation.^{3,6}

3.6. Relative Permittivity. Relative permittivity (ε') values of hydrated films were measured before and after sorption in 1 M MeOH, 1 M KOFm, or 1 M of each mix thereof (Figure 4, Supporting Information Table S5). It is

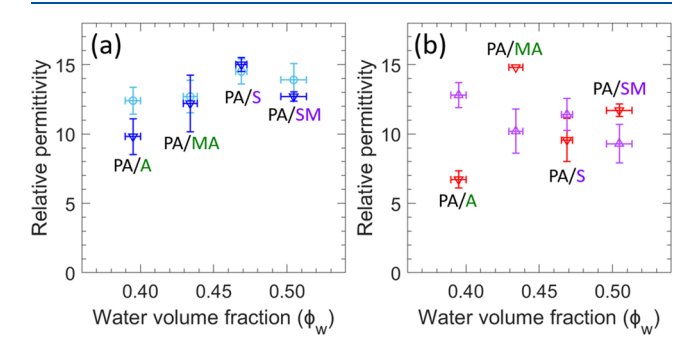


Figure 4. (a) Relative permittivity values (at 45 MHz) of all films in water (cyan) and after equilibration with 1 M MeOH (blue). (b) Relative permittivity values of all films after equilibration with 1 M KOFm (red) and a mixed solute solution containing 1 M MeOH and 1 M KOFm (purple).

useful to frame the analysis within the context of the bulk solution relative permittivity values; the relative permittivity of pure water is the highest (78⁴¹), followed by 1 M MeOH (76⁴¹), 1 M KOFm (~68, based on 0.96 M NaOFm⁴²), and 1 M of each mix thereof (~66, estimated based on both 1 M MeOH and 1 M KOFm). We expect the external solution relative permittivity properties to affect the relative permittivity properties of the membrane.²⁴ For instance, the films equilibrated with KOFm-containing solutions (i.e., 1 M KOFm and 1 M MeOH/1 M KOFm) may have lower relative permittivity values than those films equilibrated with KOFm-free solutions (i.e., pure water and 1 M MeOH).

For all films, the relative permittivity values for films equilibrated in water and 1 M MeOH were close to one another (within 10% on average), and this result may be consistent with the fact that the relative permittivity properties of water and 1 M MeOH are similar (Figure 4a). In contrast, the relative permittivity values of certain films were much more affected by equilibration with KOFm-containing solutions (i.e., 1 M KOFm or a solution containing 1 M MeOH and 1 M KOFm). For the acrylate films (PA/A and PA/S, without methacrylate backbone linkages), relative permittivity values after equilibration with 1 M KOFm were less than those before equilibration by 40% on average (Table S5, cyan and red in Figure 4b). This result is expected, as the relative permittivity properties of KOFm-containing solutions are lower than KOFm-free solutions. Alternatively, the relative permittivity values of methacrylate-based films (PA/MA and PA/SM) before sorption were close to those after equilibration with KOFm (Table S5). This result is unexpected, as the KOFm sorption coefficients of PA/MA and PA/SM were close to those of PA/A and PA/S. These observations may be consistent with a physical picture where methyl group incorporation influences polymer/solvent interactions so that KOFm does not interfere with the hydrogen bonding between the polymer and water, which leads to maintaining the relative permittivity.²⁴

In the acrylate films (PA/A and PA/S), the relative permittivity values, after equilibration with the external solution containing 1 M MeOH and 1 M KOFm, were close to those before equilibration, within 12% on average (Table S5). In contrast, the relative permittivity values of the methacrylate films (PA/MA and PA/SM) after equilibration with the external solution containing 1 M MeOH and 1 M KOFm were less than those before equilibration by 28% on average (Table S5). This result may be due to the impact of reduced water content within the methacrylate films after sorption in the mixed solute solution. We observed that the water volume fractions within PA/MA and PA/SM, after equilibration with the mixed solute solution, were lower, by 5%, than those values after equilibration with the single solute solutions (either 1 M MeOH or 1 M KOFm). At the same time, the volume fraction for PA/A and PA/S decreased by only 2% when comparing equilibration with the mixed solute solution and the single solute solutions (Table S5).

These results suggest that polymer rigidity (i.e., methyl group incorporation) may impact the relative permittivity properties of the swollen polymers, especially in the mixed organic solute solution. Moreover, these results suggest that relative permittivity values of hydrated films can be a valuable tool to investigate the influence of sorbed organic solutes on material properties.

4. CONCLUSIONS

The single and mixed solute transport of two CO_2 reduction products, methanol (MeOH) and formate (OFm⁻), were investigated in four different phenyl acrylate (PA)-based cross-linked ion exchange membranes (PA/A, PA/MA, PA/S, and PA/SM). Briefly, PA/A and PA/MA are anion exchange membranes with QA⁺ functional groups and PA/S and PA/SM are cation exchange membranes with SO_3 functional groups, where PA/A and PA/S are methacrylate-free films, while PA/MA and PA/SM are methacrylate-containing films. In mixed solute permeation experiments, we observed MeOH tends to permeate more rapidly than KOFm at a lower water volume

fraction, presumably due to the flux coupling. In mixed solute sorption experiments, we note that PA/MA had the lowest MeOH and KOFm sorption coefficients, which is encouraging in terms of preventing the crossover of these CO2 reduction products. Finally, we hypothesized that methacrylate backbone linkages, which provide greater polymer rigidity in PA/MA and PA/SM compared to PA/A and PA/S, may influence polymer-water interactions such that KOFm does not interfere significantly with the hydrogen bond network within the material. We observed lower relative permittivity values when MeOH was present in the equilibration solution likely due to lower water content within swollen films. Based on these findings, enhancing anion exchange membranes by incorporating methacrylate monomers to increase steric hindrance (via the quaternary carbons) may be useful for engineering membranes for CO₂ reduction cells.

ASSOCIATED CONTENT

Supporting Information

The Supporting Information is available free of charge at https://pubs.acs.org/doi/10.1021/acs.jpcc.3c01854.

Glass transition temperatures; stress—strain curves; MeOH and KOFm permeability and sorption coefficients; volume fraction of solutes, water, and polymer after equilibration; relative permittivity at 45 MHz of hydrated films before and after equilibration; dielectric loss (PDF)

AUTHOR INFORMATION

Corresponding Author

Bryan S. Beckingham — Department of Chemical Engineering, Auburn University, Auburn, Alabama 36849, United States; orcid.org/0000-0003-4004-0755; Email: bsb0025@auburn.edu

Authors

Jung Min Kim – Department of Chemical Engineering, Auburn University, Auburn, Alabama 36849, United States; Department of Chemical Engineering, University of Virginia, Charlottesville, Virginia 22903, United States; ⊚ orcid.org/ 0000-0003-2552-5412

Yi-hung Lin — Department of Chemical Engineering, Auburn University, Auburn, Alabama 36849, United States;
orcid.org/0000-0001-9025-153X

Sean M. Bannon — Department of Chemical Engineering, University of Virginia, Charlottesville, Virginia 22903, United States

Geoffrey M. Geise — Department of Chemical Engineering, University of Virginia, Charlottesville, Virginia 22903, United States; orcid.org/0000-0002-5439-272X

Complete contact information is available at: https://pubs.acs.org/10.1021/acs.jpcc.3c01854

Notes

The authors declare no competing financial interest.

ACKNOWLEDGMENTS

This material is based upon work supported by the U.S. Department of Energy, Office of Science, Office of Basic Energy Sciences under Award No. DE-SC0021215 and is based upon work supported in part by the National Science Foundation under award CBET-1947936. Acknowledgment is

made to the Donors of the American Chemical Society Petroleum Research Fund for partial support of this research.

REFERENCES

- (1) Anwar, M. N.; Fayyaz, A.; Sohail, N. F.; Khokhar, M. F.; Baqar, M.; Khan, W. D.; Rasool, K.; Rehan, M.; Nizami, A. S. CO2 Capture and Storage: A Way Forward for Sustainable Environment. *J. Environ. Manage* **2018**, 226, 131–144.
- (2) Resasco, J.; Bell, A. T. Electrocatalytic CO2 Reduction to Fuels: Progress and Opportunities. *Trends Chem.* **2020**, 2 (9), 825–836.
- (3) Katzenberg, A.; Angulo, A.; Kusoglu, A.; Modestino, M. A. Impacts of Organic Sorbates on the Ionic Conductivity and Nanostructure of Perfluorinated Sulfonic-Acid Ionomers. *Macromolecules* **2021**, *54* (11), 5187–5195.
- (4) Baessler, J.; Oliveira, T.; Keller, R.; Wessling, M. Paired Electrosynthesis of Formic Acid from CO2 and Formaldehyde from Methanol. *Acs Sustain Chem. Eng.* **2023**, *11* (18), 6822–6828.
- (5) Wang, Z.; Parrondo, J.; Ramani, V. Anion Exchange Membranes Based on Polystyrene-Block-Poly(Ethylene-Ran-Butylene)-Block-Polystyrene Triblock Copolymers: Cation Stability and Fuel Cell Performance. *J. Electrochem. Soc.* **2017**, *164* (12), F1216—F1225.
- (6) Kim, J. M.; Lin, Y.; Hunter, B.; Beckingham, B. S. Transport and Co-Transport of Carboxylate Ions and Ethanol in Anion Exchange Membranes. *Polymers* **2021**, *13* (17), 2885.
- (7) Park, J.; Ko, Y.; Lim, C.; Kim, H.; Min, B. K.; Lee, K.-Y.; Koh, J. H.; Oh, H.-S.; Lee, W. H. Strategies for CO2 Electroreduction in Cation Exchange Membrane Electrode Assembly. *Chem. Eng. J.* **2023**, 453, 139826.
- (8) Wang, N.; Miao, R. K.; Lee, G.; Vomiero, A.; Sinton, D.; Ip, A. H.; Liang, H.; Sargent, E. H. Suppressing the Liquid Product Crossover in Electrochemical CO2 Reduction. *Smartmat* **2021**, 2 (1), 12–16.
- (9) Ramdin, M.; Morrison, A. R. T.; de Groen, M.; van Haperen, R.; de Kler, R.; van den Broeke, L. J. P.; Trusler, J. P. M.; de Jong, W.; Vlugt, T. J. H. High Pressure Electrochemical Reduction of CO2 to Formic Acid/Formate: A Comparison between Bipolar Membranes and Cation Exchange Membranes. *Ind. Eng. Chem. Res.* **2019**, *58* (5), 1834–1847.
- (10) Paul, M.; Park, H. B.; Freeman, B. D.; Roy, A.; McGrath, J. E.; Riffle, J. S. Synthesis and Crosslinking of Partially Disulfonated Poly(Arylene Ether Sulfone) Random Copolymers as Candidates for Chlorine Resistant Reverse Osmosis Membranes. *Polymer* **2008**, 49 (9), 2243–2252.
- (11) Kim, J. M.; Wang, Y.; Lin, Y.; Yoon, J.; Huang, T.; Kim, D.-J.; Auad, M. L.; Beckingham, B. S. Fabrication and Characterization of Cross-Linked Phenyl-Acrylate-Based Ion Exchange Membranes and Performance in a Direct Urea Fuel Cell. *Ind. Eng. Chem. Res.* **2021**, *60* (41), 14856–14867.
- (12) Kim, J. M.; Mazumder, A.; Li, J.; Jiang, Z.; Beckingham, B. S. Impact of PEGMA on Transport and Co-Transport of Methanol and Acetate in PEGDA-AMPS Cation Exchange Membranes. *J. Membr. Sci.* 2022, 642, 119950.
- (13) Kim, J. M.; Lin, Y.; Aravindhan, P. P.; Beckingham, B. S. Impact of Hydrophobic Pendant Phenyl Groups on Transport and Co-Transport of Methanol and Acetate in PEGDA-SPMAK Cation Exchange Membranes. *Chem. Eng. Res. Des.* **2022**, *185*, 418–429.
- (14) Kim, J. M.; Beckingham, B. S. Transport and Co-transport of Carboxylate Ions and Alcohols in Cation Exchange Membranes. *J. Polym. Sci.* **2021**, *59*, 2545–2558.
- (15) Wijmans, J. G.; Baker, R. W. The Solution-Diffusion Model: A Review. J. Membr. Sci. 1995, 107 (1-2), 1-21.
- (16) Geise, G. M.; Freeman, B. D.; Paul, D. R. Characterization of a Sulfonated Pentablock Copolymer for Desalination Applications. *Polymer* **2010**, *51* (24), 5815–5822.
- (17) Chang, K.; Xue, T.; Geise, G. M. Increasing Salt Size Selectivity in Low Water Content Polymers via Polymer Backbone Dynamics. *J. Membr. Sci.* **2018**, 552, 43–50.
- (18) Grulke, E. A.; Immergut, E. H.; Brandrup, J. *Polymer Handbook*, 4th ed.; Wiley: 2003.

- (19) Mredha, Md. T. I.; Pathak, S. K.; Tran, V. T.; Cui, J.; Jeon, I. Hydrogels with Superior Mechanical Properties from the Synergistic Effect in Hydrophobic-Hydrophilic Copolymers. *Chem. Eng. J.* **2019**, 362, 325–338.
- (20) Dobyns, B. M.; Kim, J. M.; Beckingham, B. S. Multicomponent Transport of Methanol and Sodium Acetate in Poly(Ethylene Glycol) Diacrylate Membranes of Varied Fractional Free Volume. *Eur. Polym. J.* **2020**, *134*, 109809.
- (21) Yasuda, H.; Lamaze, C. E.; Ikenberry, L. D. Permeability of Solutes through Hydrated Polymer Membranes. Part I. Diffusion of Sodium Chloride. *Makromol. Chem.* **1968**, *118* (1), 19–35.
- (22) Yasuda, H.; Peterlin, A.; Colton, C. K.; Smith, K. A.; Merrill, E. W. Permeability of Solutes through Hydrated Polymer Membranes. Part III. Theoretical Background for the Selectivity of Dialysis Membranes. *Makromol. Chem.* **1969**, *126* (1), 177–186.
- (23) Beckingham, B. S.; Lynd, N. A.; Miller, D. J. Monitoring Multicomponent Transport Using in Situ ATR FTIR Spectroscopy. *J. Membr. Sci.* **2018**, *550*, 348–256.
- (24) Chang, K.; Geise, G. M. Dielectric Permittivity Properties of Hydrated Polymers: Measurement and Connection to Ion Transport Properties. *Ind. Eng. Chem. Res.* **2020**, *59* (12), 5205–5217.
- (25) Chang, K.; Luo, H.; Bannon, S. M.; Lin, S. Y.; Agata, W.-A. S.; Geise, G. M. Methoxy Groups Increase Water and Decrease Salt Permeability Properties of Sulfonated Polysulfone Desalination Membranes. J. Membr. Sci. 2021, 630, 119298.
- (26) Luo, H.; Chang, K.; Bahati, K.; Geise, G. M. Functional Group Configuration Influences Salt Transport in Desalination Membrane Materials. *J. Membr. Sci.* **2019**, *590*, 117295.
- (27) Chang, K.; Luo, H.; Geise, G. M. Water Content, Relative Permittivity, and Ion Sorption Properties of Polymers for Membrane Desalination. *J. Membr. Sci.* **2019**, *574*, 24–32.
- (28) Lu, Z.; Lanagan, M.; Manias, E.; Macdonald, D. Dielectric Properties of Polymer Electrolyte Membranes Measured by Two-Port Transmission Line Technique. *Electrochem Soc. Transactions* **2010**, 28 (29), 95–105.
- (29) Paddison, S. J.; Bender, G.; Kreuer, K.-D.; Nicoloso, N.; Jr, T. A. Z. The Microwave Region of the Dielectric Spectrum of Hydrated Nafion (R) and Other Sulfonated Membranes. *J. New Mater. Electrochem. Systems* **2000**, *3*, 293–302.
- (30) Chang, K.; Luo, H.; Geise, G. M. Influence of Salt Concentration on Hydrated Polymer Relative Permittivity and State of Water Properties. *Macromolecules* **2021**, *54* (2), 637–646.
- (31) Luo, H.; Chang, K.; Bahati, K.; Geise, G. M. Engineering Selective Desalination Membranes via Molecular Control of Polymer Functional Groups. *Environ. Sci. Tech Let* **2019**, *6* (8), 462–466.
- (32) Kusoglu, A.; Weber, A. Z. New Insights into Perfluorinated Sulfonic-Acid Ionomers. *Chem. Rev.* **2017**, *117* (3), 987–1104.
- (33) Pei, S.-T.; Jiang, S.; Liu, Y.-R.; Huang, T.; Xu, K.-M.; Wen, H.; Zhu, Y.-P.; Huang, W. Properties of Ammonium Ion-Water Clusters: Analyses of Structure Evolution, Noncovalent Interactions, and Temperature and Humidity Effects. *J. Phys. Chem.* **2015**, *119* (12), 3035–3047.
- (34) Wu, H.; Gong, Q.; Olson, D. H.; Li, J. Commensurate Adsorption of Hydrocarbons and Alcohols in Microporous Metal Organic Frameworks. *Chem. Rev.* **2012**, *112* (2), 836–868.
- (35) Nightingale, E. R. Phenomenological Theory of Ion Solvation. Effective Radii of Hydrated Ions. *J. Phys. Chem.* **1959**, *6*3 (9), 1381–1387.
- (36) Caminiti, R.; Cucca, P.; Monduzzi, M.; Saba, G.; Crisponi, G. Divalent Metal-Acetate Complexes in Concentrated Aqueous Solutions. An X-ray Diffraction and NMR Spectroscopy Study. *J. Chem. Phys.* **1984**, *81* (1), 543–551.
- (37) Ito, M.; Kostyuk, P. G.; Oshima, T. Further Study on Anion Permeability of Inhibitory Post-synaptic Membrane of Cat Motoneurones. *J. Physiology* **1962**, *164* (1), 150–156.
- (38) Koros, W. J.; Chern, R. T.; Stannett, V.; Hopfenberg, H. B. A Model for Permeation of Mixed Gases and Vapors in Glassy Polymers. J. Polym. Sci. Polym. Phys. Ed 1981, 19 (10), 1513–1530.

- (39) Kamcev, J.; Paul, D. R.; Freeman, B. D. Ion Activity Coefficients in Ion Exchange Polymers: Applicability of Manning's Counterion Condensation Theory. *Macromolecules* **2015**, *48* (21), 8011–8024.
- (40) Manning, G. S.; Ray, J. Counterion Condensation Revisited. *J. Biomol Struct Dyn* **1998**, *16* (2), 461–476.
- (41) Albright, P. S.; Gosting, L. J. Dielectric Constants of the Methanol-Water System from 5 to 55° 1. *J. Am. Chem. Soc.* **1946**, 68 (6), 1061–1063.
- (42) Rahman, H. M. A.; Hefter, G.; Buchner, R. Hydration of Formate and Acetate Ions by Dielectric Relaxation Spectroscopy. *J. Phys. Chem. B* **2012**, *116* (1), 314–323.